Accepted Manuscript

Please cite this article as: Khan SA, Asiri AM, Al-Dies A-AnoodM, Osman OI, Asad M, Zayed MEM, One-pot synthesis, physicochemical and photophysical properties of deep blue light - emitting highly fluorescent pyrene-imidazole dye: A combined experimental and theoretical study, *Journal of Photochemistry and Photobiology, A: Chemistry* (2018), https://doi.org/10.1016/j.jphotochem.2018.06.015

One-pot synthesis, physicochemical and photophysical properties of deep blue light - emitting highly fluorescent pyrene-imidazole dye: A combined experimental and theoretical study

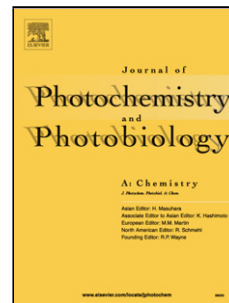Salman A. Khan[1,*], Abdullah M. Asiri[1,2,**], Al-Anood M. Al-Dies, Osman I. Osman[1], Mohammed Asad[1], Mohie E.M. Zayed[1]

[1]Department of Chemistry, Faculty of Science, King Abdulaziz University, P. O. Box 80203, Jeddah 21589, Saudia Arabia
[2]Center of Excellence for Advanced Materials Research (CEAMR), King Abdulaziz University, P. O. Box 80203, Jeddah 21589, Saudia Arabia

Correspondence Author e-mail adders: sahmad_phd@yahoo.co.in (S. A. Khan), aasiri2@kau.edu.sa (A. M. Asiri**)

Graphical Abstract:

HOMO

LUMO
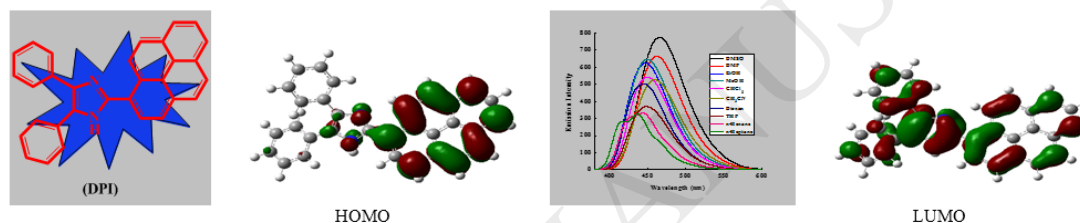
Highlights

- One pot synthesis of (4,5-diphenyl-2-(pyren-1-yl)-1*H*-imidazole (DPI)
- Spectroscopic and photophysical investigations of DPI dye
- Determine the critical micelle concentration (CMC) of CTAB and SDS
- Frontier Molecular Orbitals (FMOs) study of DPI

Abstract:

A one-pot multi-component synthesis of 4,5,-diphenyl-2-(pyren-1-yl)-1H-imidazole (DPI) chromophore was performed by the reaction of benzil, pyrene-1-carboxaldehyde and ammonium acetate in acetic acid. Structure elucidation of DPI chromophore was confirmed by spectroscopic techniques (FT-IR, ^{1}H-NMR, ^{13}C-NMR and mass spectra). The physicochemical and photophysical parameters of DPI chromophore such as extinction coefficient, oscillator strength, dipole moment, stokes shift and fluorescence quantum yield were calculated experimentally and theoretically on the basis of the different solvents polarity to see the effect of the solvents on DPI chromophore. DPI chromophore was also applicable for determination of critical micelle concentration (CMC) of cationic and anionic surfactant such as cetyl trimethyl ammonium bromide (CTAB) and sodium dodecyl sulfate (SDS).

1

1. Introduction

Over the last few decades, the synthesis of heterocyclic compounds has become a keystone of synthetic organic chemistry because of extensive multiplicity of applications of these heterocyclic compounds in the pharmaceutical and medicinal chemistry [1]. Five-member two nitrogen atoms including heterocyclic compound with special reference of imidazole normally found in many biological systems such as Olmesarten and Losartan [2]. IUPAC name of imidazole is 1,3-diaza-,2,4-cyclopentadiene. It is a planar five-member heterocyclic compound having three carbon atoms and two nitrogen atoms in positions 1 and 3. The imidazole moiety is an important pharmaphore that embraces a number of pharmacological behaviors such as antifungal, antibacterial [3], anticancer [4], anti-inflammatory and antitumor etc. [5, 6]. It is also significantly applicable in the chemical analytical field such as polymer stabilizer [7], laser dye [8], environmental probes in bio-molecules [9] and Raman filters [10]. The long π-bond conjugated system of the chromophores is responsible for their colour by absorbing the UV-light at certain wavelength. The Imidazole nucleus containing the long π-bond conjugated system are applicable in various fields of materials science such as Organic light-emitting diodes (OLED) [11, 12], dye-sensitized solar cells (DSSC) [13], chemosensors for the detection of metal ions [14] and optoelectronic devices [15]. The photophysical and physicochemical parameters of the imidazole containing chromophore such as oscillator strengths, extinction coefficients, stokes shift, dipole moments and fluorescence quantum yields are important parameters that prove the physical behavior of the chromophores [16]. On the basis of literature survey, we found, lot of work have been done on imidazole derivative with their various biological applications and also in the area of material

2

sciences, but no one reported synthesis of imidazole as a donor-acceptor chromophore, our aim to design highly fluorescence and highly photostable long pi bond conjugated system containing with donor and acceptor chromophore can be use as organic light emitting diode. In this manuscript we are reporting synthesis of 4,5-diphenyl-2-(pyren-1-yl)-1H-imidazole (DPI) chromophore by the one-pot reaction of benzil, pyrene-1-carboxaldehyde and ammonium acetate. The physicochemical and photophysical properties such as extinction coefficients, stokes shifts, oscillator strengths, dipole moments and fluorescence quantum yields of the chromophore in different solvents on the basis of the polarity were determined experimentally. Density Functional Theory (DFT) was also used to accompaniment the experimentally physical behavior of the newly synthesized molecule.

2. Experimental

2.1. Chemicals and reagents

All the chemical and reagents for this experiment like pyrene-1-carboxaldehyde, benzil, ammonium acetate and acetic acid were obtained from Acros Organic. All solvents were used HPLC grade.

2.2. Apparatus

The reaction was examined by 0.2 mm silica gel (60F-254) coated thin layer chromatography. Melting point of DPI dye was determined by using a Stuart Scientific Co. Ltd apparatus. The IR spectra of the compound (DPI) was measured by a Perkin Elmer FT-IR spectrometer. NMR spectra (^{1}H & ^{13}C) of the compound was measured by a 850MHZ Bruker AVANCE™ III HD. Mass spectra were measured by using Direct Analysis in Real Time (DART) on a JOEL AccuToF LC-plus JMS–T100LP, time-of-flight mass spectrometer (DART-ToF MS). Absorption and emission spectra DPI dye

was recorded in different solvent by Shimadzu UV-1650 PC spectrophotometer and Shimadzu RF 5301 PC spectrofluorophotometer using a 1 cm rectangular quart cell.

2.3. Synthesis of 4,5-diphenyl-2-(pyren-1-yl)-1H-imidazole (DPI)

DPI chromophore was prepared by one-pot reaction of pyrene-1-carboxaldehyde (4.14 g, 0.018 mol), benzil (3.0 g, 0.018 mol) and ammonium acetate (4.15 g, 0.018 mol) in acetic acid (20 ml) in a 50 ml round-bottom flask. Mixture was refluxed for 2 h at 150 ^{o}C in an oil bath. Progress of the reaction was monitored by the TLC. After complete the reaction, the reaction mixture was cooled to room temperature and precipitate was removed by filtration and 200 ml of distilled water was added to the filtrate heavy precipitate obtained filtered off, washed with water several times, dry and recrystallized from methanol and chloroform (5:5) (Scheme 1) [17].

Color: orange, shape: powder, Yield: 97%; m.p.: 299 ^{o}C; IR v_{max}/cm^{-1}: 3435 (NH stretch), 1579 (NH bend), 3036, 2953, 2923 (CH aromatic stretch), 1728 (C=N), 1603, 1443(C=C), 1355 (C-N); ^{1}H NMR (850 MHz, DMSO-d$_6$, δ_{ppm}): 13.00 (s, 1H, NH), 9.56 (d, 4H, CH$_{Aromatic}$, J = 8.9 Hz), 8.54 (d, 1H, CH$_{Aromatic}$, J = 7.4 Hz), 8.42 (d, 1H, CH$_{Aromatic}$, J = 8.6 Hz), 8.36 (t, 4H, CH$_{Aromatic}$, J = 7.6 Hz), 8.32 (d, 2H, CH$_{Aromatic}$, J = 9.6 Hz), 8.25 (dd, 1H, CH$_{Aromatic}$, J = 12.0 and 8.7 Hz), 8.12 (t, 2H, CH$_{Aromatic}$, J = 7.5 Hz), 7.69 (d, 1H, CH$_{Aromatic}$, J = 7.1 Hz), 7.63 (d, 1H, CH$_{Aromatic}$, J = 7.1 Hz), 7.48 (t, 1H, CH$_{Aromatic}$, J = 7.05 Hz), 7.42-7.37 (m, 1H, CH$_{Aromatic}$); ^{13}C NMR (213 MHz, DMSO-d$_6$, δ_{ppm}): 146.43 (C=N), 138.06, 135.73, 131.46, 131.43, 131.28, 130.87, 129.17, 129.01, 128.91, 128.81, 128.48, 128.41, 128.39, 128.30, 127.80, 127.75, 127.15, 127.02, 126.40, 126.05, 125.72, 125.25, 125.12, 124.89, 124.31 (C-aromatic); MS (DART-To FMS) m/z: exact mass 420.16 found 421.57 with a base peak at 231.08.

3. Results and discussion

4

3.1.Characterization of DPI

4,5-diphenyl-2-(pyren-1-yl)-1H-imidazole (DPI) chromophore was prepared by the one-pot reaction of benzil, pyrene-1-carboxaldehyde and ammonium acetate in acetic acid. The structure of novel DPI chromophore was confirmed by the FT-IR, ^{1}H-NMR and ^{13}C-NMR and mass spectroscopic techniques. FT-IR spectra of DPI chromophore show bands at 3435 and 1728 cm^{-1} which are characteristic to the N-H and C=N groups vibrations, respectively, with no any band 1658 cm^{-1} which is conformed that carbonyl groups of benzil and pyrene-1-carboxaldehyde are utilized for the formation of imidazole ring. The structure of DPI chromophore was further conformed by ^{1}H-NMR spectra. The ^{1}H-NMR spectra of DPI chromophore was measured in DMSO-d6, its shows a singlet peak at δ 13.00 due to presence of N-H group in imidazole ring. The ^{1}H-NMR spectra also showed doublet (d), doublet of doublets (dd), triplet (t) and multiplet (m) due to present of 19 aromatic protons (Fig. S1). ^{13}C-NMR spectra also confirmed the formation of DPI chromophore, its shows signal at δ 146.43 due to prescence of azo-carbon of the imidazole ring and signal in range of δ124.31-138.06, due to aromatic carbon. The detailed ^{13}C-NMR spectrum of the DPI chromophore is given in the experimental section. Finally, structure of DPI chromophore was confirmed by the mass spectra, its shows a molecular ion peak m/z at 421.57 with a base peak at 231.08 (Fig. S2).

3.2. Spectra behavior of DPI chromophore in different solvents

The absorbance spectra of the 4,5-diphenyl-2-(pyren-1-yl)-1H-imidazole (DPI) chromophore (1 x 10^{-5} M) were obtained in nine different polarity solvents. As shown in the Fig. 1, the polarities of the solvents have considerably affected the absorption maxima with a red shift 16 nm from n-Hexane (354 nm) to DMSO (370 nm), indicating the polar character of DPI chromophore in the ground state. As expected, red shift is

5

because of strong intramolecular charge transfer (ICT) from push to pull group (CNHC group to CNC moiety) as found in other related compounds [18].

As Fig. 2 shows, on excitation with 365 nm, the fluorescence spectrum of DPI chromophore displays a strong bathochromic shift on increasing the solvents polarity. The emission profile undergoes a red-shift of 30 nm in emission maxima from n-Hexane (440 nm) to DMSO (470 nm), indicating photoinduced intramolecular singlet excited state charge transfer (ICT); which occurs from the electron push group (CNHC group) to the electron pull group (CNC moiety). This indicates that the polarity of DPI chromophore enhances on excitation [19]. Hence, the fluorescence profile of DPI chromophore is more effective to the polarity of the solvents than in the absorption profile; signifying that the charge transfer is much significant in the excited state in comparison to the ground state; which means that the polar solvents stabilize highly dipolar excited states.

Emission spectra of different concentrations of DPI chromophore in $CHCl_3$ were also measured exhibited almost same fluorescence maxima, only emission intensity changed with the concentration (Fig. 3).

The absorption and emission energy (E_a and E_f) of DPI chromophore in various solvents are associated with the empirical Dimroth polarity parameter $E_T(30)$ of the solvents (Fig. 4) [20]. Energy of the absorption and emission of DPI chromophore versus polarity of the various solvents was find linear correlation (Eqs. 1 and 2). Polar aprotic solvents such as DMSO and DMF shows away from the averaged line indicating that the nature of the emitting state is different for this class of solvents. A linear association between the energy of the absorption and emission versus polarity of various solvent was obtained (Eqs. 1 and 2).

$$E_a = 84.05 - 0.038 \times E_T(30) \qquad\qquad (1)$$

6

$E_f = 66.82 - 0.083 \times E_T(30)$ (2)

The solvatochromic behavior of the DPI chromophore based on the linear correlation between absorption and emission maxima (λ_{ab} and λ_{em}) and polarity solvent functions is well-known for determining excited and ground state dipole moments. Lippert-Mataga Eqs. (3) and (4), were used to determine the energy difference between the ground and excited states i.e. Stokes shift and change in dipole moment between the excited singlet and ground state [21].

$$\Delta \bar{v}_{st} \quad = \quad \frac{2(\mu_e - \mu_g)^2}{hca^3} \Delta f + Const.$$ (3)

$$\Delta f \quad = \quad \frac{\varepsilon - 1}{2\varepsilon + 1} - \frac{n^2 - 1}{2n^2 + 1}$$ (4)

where (Δv_{st}) is the stokes shift, which increases with increasing the polarity of the solvents, h is Planck's constant, c is the speed of light, a is the Onsager cavity radius, n is the refractive index of the solvent and ε is the dielectric constant. The Onsager cavity radius was taken as 5.6 A^o. Fig 5 shows the plot of the orientation polarizability of the solvents versus Stokes shift of DPI chromophore in different solvent (Δf). Change in dipole moments ($\Delta \mu$) were calculated between the singlet excited and ground states from the slop plot of orientation of polarizability of the different solvent and Stokes shift (Δv) of the DPI chromophore in different solvents and found 8.27 Debye, Positive value indicating that the excited sate is more polar than the ground state.

The transition dipole moment (μ_{12}) and oscillator strength (f) of electronic transition for DPI chromophore from ground to excited singlet state ($S_o \rightarrow S_1$) in different solvent were calculated by using the following equations (5, 6) [22].

$$f \quad = \quad 4.32 \times 10^{-9} \int \varepsilon(\bar{v}) \, d\bar{v}$$ (5)

7

$$\mu_{12}{}^2 \quad = \quad \frac{f}{4.72 \times 10^{-7} \, E_{max}} \tag{6}$$

where v is the wavenumber measured in cm^{-1}, ε is the numerical value for molar extinction coefficient is measured in dm^{-3} mol^{-1} cm^{-1} and E_{max} is the energy the maximum absorption band in cm^{-1}. Calculated value of transition dipole moment and oscillator strength are listed in the table 1, which designate that the transition $S_o \rightarrow S_1$ is strongly allowed.

The empirical Dimroth polarity parameters, E_T (30) and E_T^N of DPI chromophore were calculated according to the following equations [23].

$$E_T^N = \frac{E_T(solvent) - 30.7}{32.4} \tag{7}$$

$$E_T(solvent) = \frac{28591}{\lambda_{max}} \tag{8}$$

where (λ_{max}) corresponds to the peak wavelength (nm) in the red region of the of the intramolecular charge transfer absorption of DPI chromophore. The red (bathochromic) shift from n-Hexane to DMSO designates that the photoinduced intramolecular charge transfer (ICT) arises in the singlet state, and the polarity of DPI, chromophore therefore, increases on excitation.

3.3. Fluorescence quantum yield

The fluorescence quantum yield (Φ_f) of the DPI chromophore was calculated in different solvents with the reference of fluoresce dye solution (Φ_f 0.95 in 0.1 NaOH) as stranded dye. The following equation (Eq. 9) has been applied for the calculated of fluorescence quantum yield (Φ_f).

$$\Phi_f \quad = \quad \Phi_r \frac{I \, x \, A_r \, x \, n^2}{Ir \, x A \, x n^2{}_r} \tag{9}$$

8

Where Φ_f is the fluorescence quantum yield of DPI chromophore, Φ_r is the fluorescence quantum yield of the reference dye (fluoresce), A is the absorbance at the excitation wavelength, I is the integrated fluorescence intensity and n is the refractive index of the solvent. The subscript r refers to the reference fluorescence of a known quantum yield [24].

The fluorescence quantum yields (Φ_f) of DPI chromophore have been calculated in different solvents and the values are mentioned in the table 1. The polarity of the solvents strongly affected on the value of the fluorescence quantum yields of DPI chromophore. Additionally, the fluorescence quantum yield of DPI chromophore in different solvents and their relationships with the $E_T(30)$ of the various solvents are shown in Fig 6, where $E_T(30)$ is the solvent polarity factor recognized by Reichardt. As presented in the table 1, the fluorescence quantum yield of DPI chromophore increases with increasing polarity of the solvent; which increases from 0.40 in n-Hexane to 0.68 in DMSO (a non-polar solvent to highly polar solvent). This result is associated to the prevalence of negative solvatokinetic effect (n-Hexane to DMSO) [25]. One main reason for the negative solvatokinetic (the increase of Φ_f is accompanied by a appropriate enhancement of intramolecular charge transfer) could be due to the biradicaloid charge transfer involving the un-bridged double bonds and the other cause could be related to the proximity effect for a chromophore with n-π^* and π-π^* electron configuration. In other words, in non-polar solvents, these effects will result in effective non-radiative decay of the excited states.

3.4. Effect of surfactant on emission spectrum of DPI

Due to pyrene carboxaldehyde well-known probes for the deamination of the CMC of CTAB, pyrene containing imidazole (DPI) can be applicable to determine the CMC of the surfactants. Two surfactants namely sodium dodecyl sulphate (SDS) and cetyl trimethyl ammonium bromide (CTAB) surfactants as an anionic and cationic surfactant were chosen for estimated the emission behavior of the DPI chromophore. The two specified surfactants were selected because the ionic charges possessed by DPI chromophore can be influenced by the negatively charged SDS and the positively charged CTAB. Thus, the charge attraction accounts for the DPI chromophore fluorescence behavior. The fluorescence emission spectra of DPI chromophore in the absence and presence of SDS and CTAB were measured. The fluorescence intensity of DPI chromophore decreases with an increase of the SDS concentration (2×10^{-3} up to 1.8×10^{-2} M). Moreover, reductions that are more significant, noticed in fluorescence intensities of DPI with SDS. The quenching of emission intensity of DPI chromophore upon increasing SDS concentration can likely be recognized to the association of DPI chromophore with SDS. It can be observed that there was a successive decrease in the relative fluorescence intensity of DPI chromophore with an increase in the SDS concentration, strongly providing that there was an interaction between DPI and SDS Fig. 7. The emission intensity of DPI chromophore increases with increasing the concentration of CTAB from 2×10-4 up to 1.8×10^{-3} M. Such enhancement in the emission intensity of 1×10^{-5} M DPI chromophore at fixed concentrations with an increase in the CTAB concentration may likely be ascribed to the association mechanism of DPI chromophore with CTAB Fig. 8. It seems that the DPI dye molecule are located in the hydrocarbon core of CTAB aggregates, while in SDS they are located at the micelle-water interface, with quenching role of water [26]. The emission intensity of DPI chromophore decreases with increasing concentration of surfactant SDS and

10

increases with increasing concentration of surfactant CTAB, with an abrupt change in emission intensity occurring at surfactant concentration of 6.79×10^{-3} and 9.51×10^{-4} mo dm^{-3} which are very close to the critical micelle concentration (CMC) of SDS and CTAB (Fig. 9 and 10) [27]. Thus, DPI chromophore can be employed as a probe and quencher to determine the CMC of the surfactants.

3.5. Fluorescence quenching of DPI with ethylene glycol

The fluorescence quenching of DPI chromophore in dioxan was studied by using polar protic solvent ethylene glycol as quenchers Fig. 11. As follows from these figure, the fluorescence spectra undergo very complex changes on adding different concentration of ethylene glycol, i.e., the emission intensity of DPI chromophore decreases with increasing the concentration of ethylene glycol and also shifted to longer wavelength, possess changed half widths and band profiles of the emission spectrum. This behavior indicates, that in such a solution an extra factor contributes to the well-known dipole-dipole interaction, i.e., hydrogen-bonding interactions between the ethylene glycol molecule and imidazole group of DPI chromophore, not only in the molecule and ethylene glycol, not only in the S_0 state, but also in the excited, S_1, state [28]. The Stern–Volmer constants (K_{SV}) was calculated from the Stern– Volmer plots shown in Fig 12. The K_{SV} constant was determined as 0.40 M^{-1} in ethylene glycol. The dependence of fluorescence characteristics on ethylene glycol properties suggest a potential application of DPI chromophore to probe of the polarity and hydrogen bonding properties of its local microenvironment.

$$I_0 / I_f = 1 + K_{sv} [Q] \tag{10}$$

11

where I_o and I_f are the relative integrated fluorescence intensities without and with the quencher concentration [Q] and K_{sv} (Stern-Volmer constant).

3.6. DFT Calculations

The molecular structure of DPI chromophore was optimized using the long-range corrected (LC) column-attenuating (CAM) method of the hybrid Becke's three parameter Lee-Young-Parr correlation functional (CAM-B3LYP) [29] of the density functional theory (DFT) with double-zeta and polarization functions on heavy atoms basis set [6-31+G*]. A global minimum on the potential energy profile of DPI was located and evidenced by the absence of any imaginary vibrational wavenumber. Time-Dependent density functional theory (TD-DTF) [30] and the polarizable continuum model (PCM) method [31] with the 6-31+G* basis set were applied to simulate the Ultra-Violet spectra of DPI in n-Hexane (C_6H_{12}), chloroform ($CHCl_3$), tetrahydrofuran (THF), ethanol (C_2H_5OH), methanol (CH_3OH), acetonitrile (CH_3CN) and dimethyl sulphoxide (DMSO). All these calculations were performed using the Gaussian09 Suites of program [32] together GaussView [33] for monitoring the geometry of DPI chromophore. Version 3.1 of natural bond orbital (NBO) program [34] was applied to compute the electric charges and hyperconjugative energies of DPI chromophore.

3.7. Geometry

Table 2 lists a few bond lengths and angles of the optimized structure of the gas-phase molecule DPI chromophore that is depicted by Fig.13. They are computed by using CAM-B3LYP/6-31+G* level of theory. It is worth extracting some geometrical remarks from Table 2 in conjunction with Fig.13: (1) the pyrene and imidazole rings are out-of-plane by *ca.* 37° as shown by the dihedral angle N5-C1-C7-C8, (2) the dihedral angles N5-C4-C32-C33 and C4-C3-C43-C45 indicate that the two benzene rings are off-plane with the imidazole ring by *ca.* 30° and 44°, respectively, (3) All

12

carbon-carbon bonds are doubly bonded or partially multiply bonded. This feature does not exclude even C1-C7, C3-C4, C3-C43 and C4-C32 bond lengths being shorter than expected by 0.064, 0.065, 0.065 and 0.061Å, respectively, compared to the typical C-C single bond of ethane [35], (4) the computed bond angles of 105°-129° show clearly the sp^2 hybridization scheme over the entire macromolecule.

3.8. UV-Visible Spectra

The π→π* and n→π* electronic transitions from the higher occupied molecular orbitals (HOMO) to the lower unoccupied molecular orbitals (LUMO), collectively called frontier molecular orbitals (FMOs) lead to UV-Vis. absorption spectra of π-conjugated organic molecules [36]. The macromolecule DPI has many double bonds and lone pairs on the nitrogen atoms. Table 3 lists the experimental UV-Vis. absorption and emission electronic transitions of DPI chromophore in different solvents as mention in table 3 together with their theoretical peers computed by using PCM/TD-CAM-B3LYP/6-31+G* level of theory. Overall, excellent agreement between the experimental and simulated absorption and emission wavelength maxima is obtained. On the one hand, the absorption maximum wavelengths are theoretically underestimated. The discrepancy between the experimental and estimated maximum wavelengths increases from *ca.* 7nm in n-Hexane to *ca.* 24nm in DMSO. On the other hand, the emission wavelength maxima are overvalued compared to their measured analogues. The variance between them does not exceed *ca.* 25nm. It is worth mentioning that the estimated maximum absorption wavelengths are gradually blue-shifted while the emission wavelength maxima are progressively red-shifted with the increase of solvent polarity. The non-linear dependence of solvatochromic shifts of the absorption maxima and their oscillator strengths on the dielectric constant of the solvents could be explained in terms of the intermolecular hydrogen bonds between solute and solvent

13

[37]. The interaction between the solvent and solute could explain the slight fluctuations in the computed absorption wavelength maxima [38].

In Table 4 are registered the property parameters [39] of the solvents used for the solvation of DPI chromophore together with the calculated absorption maxima in these solvents. It is clear that the calculated absorption wavelengths do not correlate with the solvent polarity scale [$E_T(30)$] as the later does not include the hydrogen-bond acceptor (HBA) beside both the hydrogen–bond donor (HBD) and solvent dielectric constants [40]. Likewise the solvent polarity parameter (Δf) alone is not adequate for pinpointing the solvatochromic behaviour of DPI in the elected solvents. These two observations indicate that specific solute-solvent interactions prevail in the solvation of DPI chromophore [41]; which necessitate the use of a multiparametric solvatochromic scale of Kamlet and Taft [42,43].

As shown in Table 4, the absorption wavelength is blue-shifted of 3.2nm in going from a nonpolar n-hexane (α=0.00, β=0.00, π*=-0.4) to the acetonitrile (α=0.19, β=0.40, π*=0.75) as the latter being highly polar and a good HBA, on the one hand. On the other hand, a blue shift of 3.4nm occurs in going from n-hexane to methanol (α=0.98, β=0.66, π*=0.60) as a result of a large HBD ability and moderate HBA and polar abilities. The anomalous solvatochromic behaviour of DPI chromophore in DMSO (α=0.00, β=0.76, π*=1.00) is attributed to its high ability as a HBA together with its relatively high polarity.

The mapped electrostatic potential for excited and ground states of the DPI chromophore applying HF/321G level of theory is depicted in Fig.14. The figure shows clearly that around the CNC moiety (acceptor) an intensive negative charge is built up; while around the CNHC group (donor) a denser positive charge is intensified in both the ground and excited states. These theoretical judgments support our experimental

14

findings that DPI chromophore could be used for the determination of the critical micelle concentrations of both SDS and CTAB surfactants.

3.9.Frontier Molecular Orbitals (FMOs)

Fig.15 depicts the gas-phase DPI frontier molecular orbitals (FMOs). CAM-B3LYP/6-31+G* level of theory was applied to compute them. On the one hand, the HOMO is localized mainly over the imidazole ring and the two adjacent phenyl groups as π-bonding orbitals (donor orbital). On the other hand, the LUMO extends entirely over the pyrene ring as π^*-antibonding orbital (acceptor orbital). This situation facilitates the intramolecular charge transfer (ICT) within the macromolecule. A detailed description of the ICT will be presented in a separate section devoted to natural bond orbital (NBO) analysis.

Table 5 lists the HOMO and LUMO energies of the solvated DPIs, together with their energy gaps (E.G.). The later parameters could be used as measures for the intermolecular solute-solvent charge transfer. As Table 4 shows energy gaps of 5.648-5.681eV which could easily ease the $\pi \rightarrow \pi^*$ and $n \rightarrow \pi^*$ charge transfer and, therefore, could evidently generate UV-Vis. spectra. It is noteworthy that the energy gaps of the solvated DPI chromophore a directly related to their nature (protic or aprotic) and/or polarities, *i.e.* their dielectric constants. These effects steadily stabilize both the HOMOs and LUMOs by varying degrees and, therefore, result in incremental small increases of the energy gaps.

The electronic chemical potential (μ) that indicates the motion of electrons in a chemical species [44], the chemical hardness (η) that examines the stability and reactivity of a chemical species [45] and the global electrophilicity index (ω) that estimates the stabilizing energy when a chemical species accepts additional electronic charge from the medium [46] are listed in Table 5. As Table 5 shows the magnitudes

15

of η and μ indicate that DPI chromophore in DMSO is the hardest, most stable and least reactive amongst the solvated chromophore, while being the softer, least stable and most reactive in n-Hexane. In addition, the ω values show that the solvation of DPI by DMSO fabricates the strongest electrophile amongst the solvated DPIs, compared to being the weakest electrophile (or a nucleophile) when solvated by n-Hexane [47].

3.10. Natural Bond Orbital Analysis

The Natural Bond Orbital (NBO) analysis [48] has gained wide endorsement in dealing with hyperconjugative interactions [49]. This is accomplished through analyzing second order perturbation energies ($E_{(2)}$) given by the relation:

$$E_{(2)} = \Delta E_{ij} = q_i (F_{ij})^2 / \Delta \varepsilon \qquad (11)$$

where F_{ij} is the NBO Kohn-Sham off-diagonal matrix elements, q_i is the occupancy of the donor orbital(i), and $\Delta \varepsilon$ is difference between the energies of the donor orbital (i) and an acceptor orbital (j). Table 6 registers the second order perturbation ($E_{(2)}$) hyperconjugative energies of DPI chromophore in the gas-phase that trace the charge transfer from the donor imidazole ring to the pyrene ring acceptor. They were computed by employing HF/321G/CAM-B3LYP/6-31+G* level of theory. They are classified as $\pi \rightarrow \pi^*$, $\sigma \rightarrow \sigma^*$ and $n \rightarrow \pi^*$ electronic charge transfer interactions. The $\pi \rightarrow \pi^*$ and $n \rightarrow \pi^*$ hyperconjugative interactions are most effective and availed totals of 174.24 and 148.61 kcal/mol, respectively; whereas the $\sigma \rightarrow \sigma^*$ transitions are extremely weak and contributed only 18.04 kcal/mol to the stabilization of the DPI chromophore. The DPI chromophore substrate intramolecular weak charge transfers from the imidazole moiety toward the phenyl groups are shown by the $\sigma_{C4-N5} \rightarrow \sigma^*_{C32-C34}$, $\sigma_{C4-N5} \rightarrow \sigma^*_{C3-C43}$, $\pi_{C3-C4} \rightarrow \pi^*_{C32-C34}$ and $\pi_{C3-C4} \rightarrow \pi^*_{C43-C44}$ interactions which stabilized DPI chromophore by 1.44, 4.66, 11.72 and 9.26 kcal/mol, respectively. Comparatively, large charge is also transferred from the imidazole ring at the pyrene moiety. These are symbolized by the

16

$\pi_{C1-N5} \to \pi^*_{C7-C9}$, $\pi_{C7-C9} \to \pi^*_{C8-C10}$, $\pi_{C8-C10} \to \pi^*_{C14-C19}$ and $\pi_{C14-C19} \to \pi^*_{C20-C24}$ transitions which availed 8.64, 36.46, 31.62 and 37.99 kcal/mol to the stabilization of the studied macromolecule. These results are in excellent agreement with our observed UV-Vis. spectra and are properly correlated with our theoretical predictions mentioned earlier.

4. Conclusion

Novel 4, 5-diphenyl-2-(pyren-1-yl)-1H-imidazole (DPI) chromophore was prepared by one-pot equimolar reaction of benzil, pyrene-1-carboxaldehyde and ammonium acetate in acetic acid. Structure of the synthesized DPI chromophore was confirmed by spectroscopic techniques and elemental analysis together with DFT study, Experimental and theoretical absorbance and emission spectra of DPI chromophore showed bathochromic shifts with increasing polarities of the solvents (n-Hexane to DMSO) to gather with the polar protic and aprotic solvents. Photophysical parameters such as extinction coefficient, dipole moment, stokes shift, oscillator strength and fluorescence quantum yield of the DPI chromophore was estimated. Its affected by the polarities and types of the solvents. The DPI chromophore can be use as probe or quencher to determine the critical micelle concentration of SDS and CTAB surfactants.

17

References

[1]. Demetzos C, Angelopoulou D, Kolocouris A, Daliani I, Mavromoustakos T. Structure elucidation, conformational analysis and thermal effects on membrane bilayers of an antimicrobial myricetin ether derivative. J Heterocyc. Chem., 2001; 38: 703-710.

[2]. Grimmett MR. Imidazole and Benzimidazole Synthesis.1997, Academic Press.

[3]. Khabnadideh S, Rezaei Z, Khalafi-Nezhad A, Bahrinajafi R, Mohamadi R, Farrokhroz AA. Synthesis of N-Alkylated Derivatives of Imidazole as Antibacterial Agents. Bioog. Med Chem. Lett., 2003; 13: 2863–2865

[4]. Schemeth D, Kappacher C, Rainer M, Thalinger R, Bonn GK. Comprehensive evaluation of imidazole-based polymers for the enrichment of selected non-steroidal anti-inflammatory drugs, Talanta 2016; 153: 177–185.

[5]. Alkahtani HM, Abbas AY, Wang S. Synthesis and biological evaluation of benzo[d] imidazole derivatives as potential anti-cancer agents. Bioorg. Med. Chem. Lett. 2012; 22: 1317-1321.

[6]. Zhou J, Ji M, Zhu Z, Cao R, Chen X, Xu B. Discovery of 2-substituted 1H-benzo[d]immidazole-4-carboxamide derivatives as novel poly (ADP-ribose) polymerase-1 inhibitors with in vivo anti-tumor activity. Eur. J. Med. Chem. 2017; 132: 26-41

[7]. Shirin-Abadi AR, Darabi A, Jessop PG, Cunningham MF. Preparation of red ispersible polymer latexes using cationic stabilizers based on 2-dimethylaminoethyl methacrylate hydrochloride and 2,20 -azobis [2-(2-imidazolin-2-yl) propane] dihydrochloride. Polymer, 2015; 60:1-8.

[8]. Samarkina DA, Gabdrakhmanov DR, Lukashenko SS, Khamatgalimov AR, Kovalenko VI, Zakharova LY. Cationic amphiphiles bearing imidazole fragment: From aggregation properties to potential in biotechnologies. Colloids Surf. A 2017; 529: 990–997

[9]. Uslu A, Tumay SO, Şenocak A, Yuksel F, Ozcan E, Yeşilot S. Imidazole/benzimidazole-modified cyclotriphosphazenes as highly selective fluorescent probes for Cu^{2+}: synthesis, configurational isomers, and crystal structures Dalton Trans., 2017; 46: 9140-9156

[10]. Cao P, Gu R, Tian Z. Surface-Enhanced Raman Spectroscopy Studies on the Interaction of Imidazole with a. Silve electrode in acetonitrile solutions, J. Phy. Chem., B: 2003; 107: 769-777.

[11]. Liu Y, Bai Q, Li J, Zhang S, Zhang C, Lu F, Yang B, Lu P. Efficient pyrene-imidazole derivatives for organic light-emitting diode. RSC Adv., 2016; 6: 17239.

[12]. Shan T, Liu Y, Tang X, Bai Q, Gao Y, Gao Z, Li J, Deng J, Yang B, Lu P, Ma Y. Highly Efficient Deep Blue Organic Light-Emitting Diodes Based on Imidazole: Significantly Enhanced Performance by Effective Energy Transfer with Negligible Efficiency Roll-off, ACS Appl. Mater. Interfaces, 2016; 8: 28771–2877.

[13]. Kumar D, Thomas KRJ, Lee C, Ho KC. Organic Dyes Containing Fluorene Decorated with Imidazole Units for Dye-Sensitized Solar Cells J. Org. Chem. 2014; 79: 3159−3172.

[14]. Zeng Q, Cai P, Li Z, Qin J, Tang BZ. An imidazole-functionalized polyacetylene: convenient synthesis and selective chemosensor for metal ions and cyanide.Chem. Commun., 2008;0: 1094–1096.

[15]. Kulhanek J, Bures F. Imidazole as a parent π-conjugated backbone in charge-transfer chromophores Beilstein J. Org. Chem. 2012; 8: 25–49.

[16]. Feng K, Hsu FL, Veer DVD, Bota K, Bu XR. Tuning fluorescence properties of imidazole derivatives with thiophene and thiazole. Journal of Photochem. Photobio. A: 2004; 165: 223–228.

[17]. Asiri AM, Baghaffar GA, Badahdah KO, Al-Sehemi AGM, Khan SA, Bukhar BA. Multifunctional switches based on bis-imidazole derivative. J. Chem. Sci.,2009; 121: 983–987.

[18]. Nad S, Kumbhakar M, Pal H. Photophysical Properties of Coumarin-152 and Coumarin-481 Dyes: Unusual Behavior in Nonpolar and in Higher Polarity Solvents. J. Phys. Chem. A 2003; 107: 4808

[19]. Willard DM, Riter RE, Levinger NE. Dynamics of polar solvation in lecithin/water/cyclohexane reverse micelles, J. Am. Chem. Soc. 1998;120: 4151–4160.

[20]. Suppan P. Invited review solvatochromic shifts: The influence of the medium on the energy of electronic states, 1990; 50: 293-330.

[21]. Lakowicz JR. Principles of Fluorescence Spectroscopy, 3rd Edn. Springer, New York, 2006.

[22]. Carlotti B, Flamini R, Kikas I, Mazzucato U, Spalletti A. Intramolecular charge transfer, solvatochromism and hyperpolarizability of compounds bearing ethenylene or ethynylene bridges. Chem Phys. 2012; 407:9–19.

19

[23]. Jonquires A, Roizard D, Cuny J, Lochon P. Solubility and polarity parameters for assessing pervaporation and sorption properties. A critical comparison for temary systems alcohol/ether/polyurethaneimide, J Membrane Science 1996; 121: 117-133.

[24]. Wurth C, Grabolle M, Pauli J, Spieles M, Resch-Genger, U. Comparison of Methods and Achievable Uncertainties for the Relative and Absolute Measurement of Photoluminescence Quantum Yields. *A*nal. Chem.*,* 2011; 83: 3431–3439.

[25]. Rurack K, Dekhtyar ML, Bricks JL, Resch-Genger U, Rettig W. Quantum Yield Switching of Fluorescence by Selectively Bridging Single and Double Bonds in Chalcones: Involvement of Two Different Types of Conical Intersections. J. Phys. Chem. A 1999; 103: 9626-9635.

[26]. Vasu AK, Kanvah S. Red-emitting cationic fluorophore as a probe for anionic surfactants Dyes Pigm,2017; 142: 230-236.

[27]. Mukherjee K, Moulik SP, Mukherjee DC. Thermodynamics of micellization of Aerosol OT in polar and nonpolar solvents. A calorimetric study. Langmuir 1993; 9: 1727-1730.

[28]. Liu YH, Li P. Excited-state hydrogen bonding effect on dynamic fluorescence of coumarin 102 chromophore in solution: A time-resolved fluorescence and theoretical study. J. Lumin., 2011; 131: 2116-2120 .

[29]. Yanai T, Tew DP, Handy NCA. A new hybrid exchange–correlation functional using the Coulomb-attenuating method (CAM-B3LYP) Chem. Phys. Lett. 2004; 393: 51-57.

[30]. Gross EKU, Kohn W. Time-Dependent Density-Functional Theory Adv. Quant. Chem. 1990; 21:255-291.

[31]. Cances E, Mennucci B, Tomasi J. A new integral equation formalism for the polarizable continuum model: Theoretical background and applications to isotropic and anisotropic dielectrics J. Chem. Phys.1997; 107: 3032-3041.

[32]. Gaussian 09, Revision A.02, Frisch, MJ, Trucks GW, Schlegel HB, ScuseriaGE, Robb MA, Cheeseman JR, Scalmani G, Barone SV, Mennucci B, Petersson GA, Nakatsuji H, Caricato M, Li X, Hratchian HP, Izmaylov AF, Bloino J, Zheng G, Sonnenberg JL, Hada M, Ehara M, Toyota K, Fukuda R, Hasegawa J, Ishida M, Nakajima T, Honda Y, Kitao O, Nakai H, Vreven T, Montgomery JA, Peralta JE, Ogliaro F, Bearpark M, Heyd JJ, Brothers, E, Kudin, KN, Staroverov VN,

Kobayashi R, Normand J, Raghavachari K, Rendell A, Burant, JC, Iyengar SS, Tomasi J, Cossi M, Rega N, Millam, JM, Klene M, Knox JE, Cross JB, Bakken V, Adamo C, Jaramillo J, Gomperts R, Stratmann RE, Yazyev O, Austin AJ, Cammi R, Pomelli C, Ochterski JW, Martin RL, Morokuma K, Zakrzewski VG, Voth GA, Salvador P, Dannenberg JJ, Dapprich S, Daniels AD, Farkas O, Foresman JB, Ortiz JV, Cioslowski J, Fox DJ. Gaussian, Inc., Wallingford CT, 2009.

[33]. Frisch A, Dennington RD, Keith TA, Milliam J, Nielsen AB, Holder AJ, Hiscocks J. GaussView Reference, Version 5.0, Gaussian Inc. Pittsburgh, 2007.

[34]. Reed EA, Curtiss LA, Weinhold F. Intermolecular interactions from a natural bond orbital, donor-acceptor viewpoint, Chem. Rev.,1988; 88: 899-926.

[35]. Hirota E, Endo Y, Saito S, Duncan JL. Microwave spectra of deuterated ethanes: Internal rotation potential function and r_z structure, J. Mol. Spect. 1981; 89: 285-295.

[36]. Davis NKS, Harry MP, Anderson L. Expanding the Porphyrin π-System by Fusion with Anthracene, Org. Lett., 2008; 10: 3945–3947.

[37]. Sancho MI, Almandoz MC, Blanco SE, Castro EA. Spectroscopic Study of Solvent Effects on the Electronic Absorption Spectra of Flavone and 7-Hydroxyflavone in Neat and Binary Solvent Mixtures; Int. J Mol Sci. 2011; 12: 8895–8912.

[38]. Bayliss NS. The Effect of the Electrostatic Polarization of the Solvent on Electronic Absorption Spectra in Solution; J. Chem. Phys.1950; 18:292.

[39]. Marcus, Y. The properties of organic liquids that are relevant to their use as solvating solvents. Chem. Soc. Rev. 1993; 22: 409–416.

[40]. Reichardt, C. Solvatochromic Dyes as Solvent Polarity Indicators. Chem. Rev. 1994; 94: 2319–2358.

[41]. Shaemningwar N, Moyon, Chandra AK, Mitra S. Effect of Solvent Hydrogen Bonding on Excited-State Properties of Luminol: A Combined Fluorescence and DFT Study; J. Phys. Chem. A 2010; 114: 60–67.

[42]. Taft RW, Kamlet MJ. The solvatochromic comparison method. 2. The α-scale of solventhydrogen-bond donor (HBD) acidities. J. Am. Chem. Soc. 1976; 98: 2886–2894.

[43]. Kamlet MJ, Doherty R, Taft R, Abraham M. Linear solvation energy relationships. 26. Some measures of relative self-association of alcohols and water. J. Am. Chem. Soc. 1983; 105: 6741–6743.

[44]. Toro-Labbe A. Characterization of Chemical Reactions from the Profiles of Energy, Chemical Potential, and Hardness; J. Phys. Chem. A, 1999; 103: 4398–4403.

[45]. Pearson RG. Chemical hardness and density functional theory; J. Chem. Sci., 2005; 117 (5):369–377.

[46]. Parr RG, Szentpaly LV, Liu S, Electrophilicity Index; J. Am. Chem. Soc., 1999; 121: 1922–1924.

[47]. Chelli S, Troshin K, Mayer P, Lakhdar S, Ofial AR, Mayr H. Nucleophilicity Parameters of Stabilized Iodonium Ylides for Characterizing Their Synthetic Potential; J. Am. Chem. Soc., 2016; 138: 10304–10313.

[48]. Reed EA, Curtiss LA. F. Weinhold, Intermolecular Interactions from a Natural Bond Orbital, Donor-Acceptor Viewpoint Chem. Rev.,1988; 88:899-926.

[49]. Reed AE, Weinhold F. Natural bond orbital analysis of near-Hartree-Fock water dimer; J. Chem. Phys.1983; 78: 4066-4073.
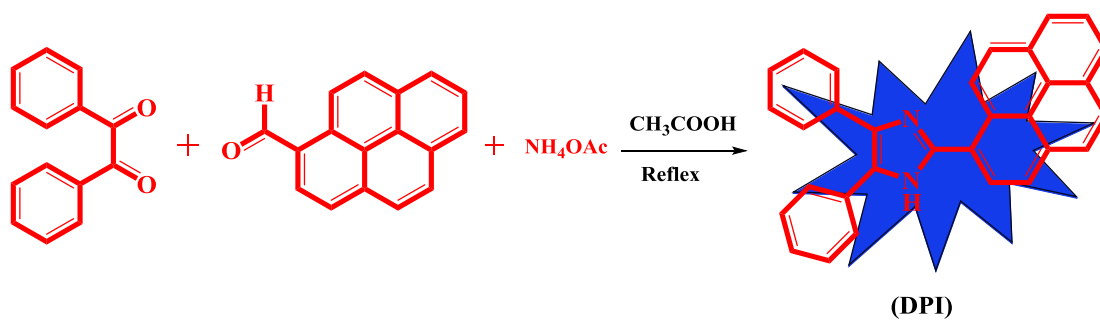
Scheme 1: Synthesis of 4,5-diphenyl-2-(pyren-1-yl)-1H-imidazole (DPI)

Table 1. Spectral data and fluorescence quantum yield (φ_f) of dye (DPI) in different solvents

Solvent	Δf	E_T^N	E_T (30) Kcal mol^{-1}	λ_{ab}(nm)	λ_{em}(nm)	ε M^{-1}cm^{-1}	f	μ_{12} Debye	$\Delta\nu_{st}$ (cm^{-1})	Φ_f
DMSO	0.263	0.441	45.1	370	470	27290	0.63	7.02	5751	0.68
DMF	0.274	0.404	43.8	368	466	27430	0.62	6.95	5714	0.56
EtOH	0.288	0.654	51.9	365	450	24000	0.49	6.15	5175	0.61
MeOH	0.308	0.762	55.4	366	453	22500	0.47	6.03	5247	0.68
CHCl$_3$	0.148	0.259	39.1	361	453	24100	0.54	6.43	5625	0.53
CH$_3$CN	0.304	0.472	45.6	367	461	22600	0.53	6.40	5556	0.54
Dioxan	0.021	0.164	36	358	448	23250	0.51	6.21	5511	0.48
THF	0.10	0.210	37.4	356	444	20000	0.44	5.76	5567	0.43
n-Hexane	0.0014	0.006	31.1	354	439	19400	0.42	5.61	5469	0.40
n-Heptane	0.0004	0.006	31.1	353	438	19080	0.41	5.47	5497	0.38

Table 2: Selected bond lengths (Å), bond angles and dihedral angles (degrees) of DPI which have been estimated by applying CAM-B3LYP/6-31+G* level of theory.

Parameter	Bond length	Parameter	Bond Angle
C1-C7	1.471	N5-C1-C7	128.5
C1-N5	1.315	N6-C1-C7	121.4
C1-N6	1.367	N5-C1-N6	110.1
N6-C3	1.379	C1-N5-C4	107.0
C3-C4	1.382	C1-N6-C3	108.5
C4-N5	1.376	N5-C4-C3	109.8
C3-C43	1.470	N6-C3-C4	104.7
C4-C32	1.474	N5-C1-C7-C8	-36.8
C32-C34	1.399	N5-C4-C32-C33	30.1
C7-C9	1.400	C4-C3-C43-C45	43.7

Table 3: The experimental UV-Vis. maximum absorption (λ_{abs}/nm) and emission (λ_{em}/nm) wavelengths for DPI in different solvents compared with the simulated ones and oscillator strengths applying TD-CAM-B3LYP/6-31+G* level of theory. Dielectric constants of solvents were also included as estimates of the polarity of solvents.

Solvent	Absorption Wavelengths			Emission Wavelengths			Dielectric Constant
	$\lambda_{expt.}$	$\lambda_{theor.}$	f	$\lambda_{expt.}$	$\lambda_{theor.}$	f	
n-Hexane	354	346.5	1.040	440	440.7	1.329	1.9
CHCl$_3$	362	345.8	1.052	451	460.7	1.499	4.8
THF	356	344.8	1.033	444	466.6	1.544	7.6
C$_2$H$_5$OH	365	343.6	1.011	450	474.7	1.601	24.5
CH$_3$OH	366	343.1	0.998	453	475.6	1.607	32.7
CH$_3$CN	367	343.3	1.003	461	475.8	1.609	37.5
DMSO	370	344.4	1.032	470	476.4	1.613	46.7

26

Table 4: The property parameters[a] of the solvents used to solvate DPI showing the polarity $E_T(30)$, the solvent polarity function (Δf), the hydrogen-bond donor (HBD) ability (α), the hydrogen-bond acceptor (HBA) ability (β), and polarity/polarizability (π^*) that affect the absorption wavelengths ($\lambda_{theor.}$) calculated by using TD-CAM-B3LYP/6-31+G* level of theory.

Solvent	E_T (30) Kcal mol^{-1}	Δf	α	β	π^*	$\lambda_{theor.}$
n-Hexane	31.1	0.0014	0.00	0.00	-0.40	346.5
CHCl$_3$	39.1	0.148	0.20	0.10	0.58	345.8
THF	37.4	0.210	0.00	0.55	0.58	344.8
C$_2$H$_5$OH	51.9	0.288	0.86	0.75	0.54	343.6
CH$_3$OH	55.4	0.308	0.98	0.66	0.66	343.1
CH$_3$CN	45.6	0.304	0.19	0.40	0.75	343.3
DMSO	45.1	0.263	0.00	0.76	1.00	344.4

a: Marcus, Y. The properties of organic liquids that are relevant to their use as solvating solvents. *Chem. Soc. Rev.* **1993**, *22*, 409–416

Table 5: The HOMO (eV), LUMO (eV) the energy gap (E.G./eV), the electronic chemical potential (μ/eV), the chemical hardness (η/eV), the global electrophilicity index (ω/eV), and the Dipole Moments (D.M./Debye) for the ground state DPI in different solvents. They have been estimated applying CAM-B3LYP/6-31+G* level of theory.

Parameter	Gas Phase	n-Hexane	CHCl$_3$	THF	C$_2$H$_5$OH	CH$_3$OH	CH$_3$CN	DMSO
HOMO	-6.513	-6.585	-6.645	-6.661	-6.683	-6.685	-6.686	-6.687
LUMO	-0.901	-0.937	-0.975	-0.987	-1.002	-1.004	-1.005	-1.006
E.G.	5.612	5.648	5.670	5.674	5.681	5.681	5.681	5.681
μ	-3.707	-3.761	-3.810	-3.824	-3.843	-3.845	-3.846	-3.847
η	2.806	2.824	2.835	2.837	2.841	2.841	2.841	2.841
ω	2.449	2.504	2.560	2.577	2.599	2.602	2.603	2.605
D.M.(g)	3.205	3.837	4.446	4.624	4.863	4.889	4.896	4.914
D.M.(ex)	---	3.418	4.045	4.233	4.483	4.510	4.518	4.537
Diff.	---	0.419	0.401	0.391	0.380	0.379	0.378	0.377

Table 6: The second order perturbation ($E_{(2)}$) estimation of the hyperconjugative energies (kcal/mol) of DPI that follow that charge transfer from the donor imidazole ring to the pyrene and phenyl rings acceptor. They were calculated using CAM-HF/321G/B3LYP/6-31+G* level of theory.

Interaction	Energy		Interaction	Energy	
$\pi_{C43-C44} \rightarrow \pi^*_{C3-C4}$	11.43		$\sigma_{C1-N5} \rightarrow \sigma^*_{C1-C7}$	3.13	
$\pi_{C3-C4} \rightarrow \pi^*_{C1-N5}$	27.12		$\sigma_{C1-C7} \rightarrow \sigma^*_{C7-C8}$	4.87	
$\pi_{C1-N5} \rightarrow \pi^*_{C7-C9}$	8.64		$\sigma_{C1-C7} \rightarrow \sigma^*_{C7-C9}$	3.94	18.04
$\pi_{C7-C9} \rightarrow \pi^*_{C8-C10}$	36.46	174.24	$\sigma_{C4-N5} \rightarrow \sigma^*_{C32-34}$	1.44	
$\pi_{C8-C10} \rightarrow \pi^*_{C14-C19}$	31.62		$\sigma_{C4-N5} \rightarrow \sigma^*_{C3-C43}$	4.66	
$\pi_{C14-C19} \rightarrow \pi^*_{C20-C24}$	37.99		$n_{1N5} \rightarrow \sigma^*_{C1-N6}$	10.72	
$\pi_{C3-C4} \rightarrow \pi^*_{C32-C34}$	11.72		$n_{1N6} \rightarrow \pi^*_{C1-N5}$	81.64	148.61
$\pi_{C3-C4} \rightarrow \pi^*_{C43-C44}$	9.26		$n_{1N6} \rightarrow \pi^*_{C3-C4}$	56.25	

29
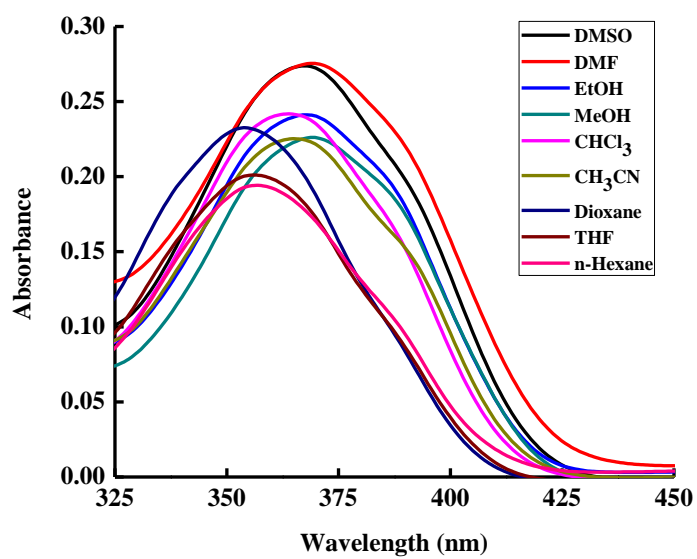
Fig. 1. Electronic absorption spectra of 1×10^{-5} mol dm^{-3} of DPI in different solvents.
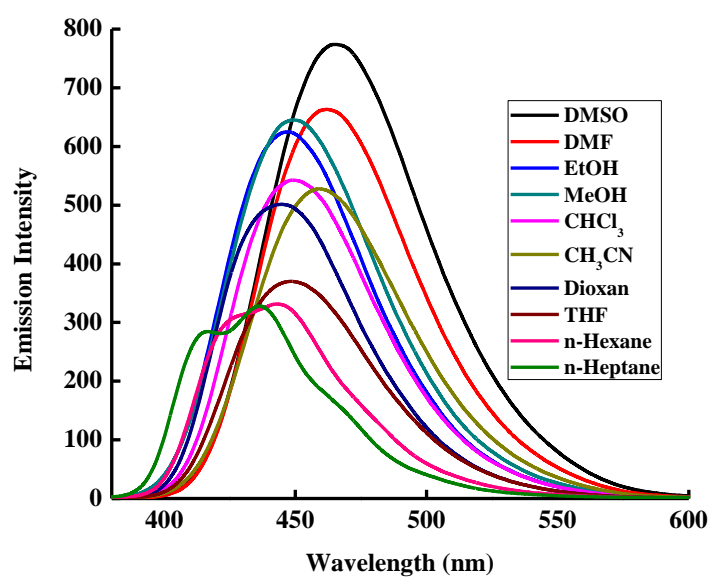
Fig. 2. Emission spectra of 1×10^{-5} mol dm^{-3} of DPI in different solvents.

31
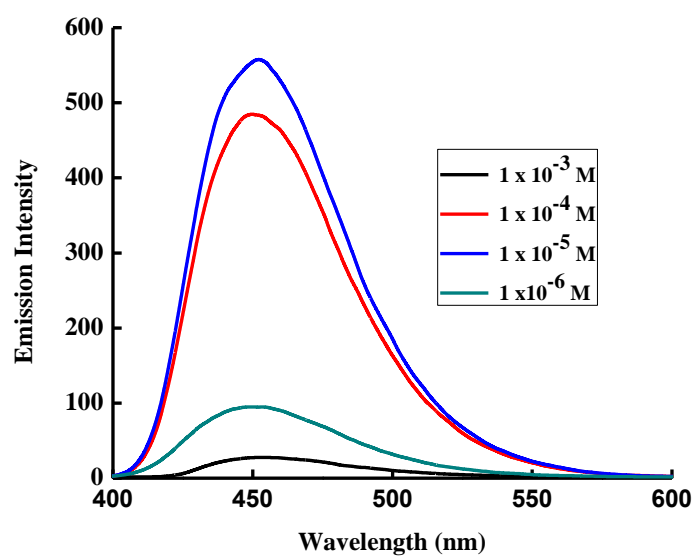
Fig. 3. Emission spectra of different concentration of DPI in CHCl$_3$.
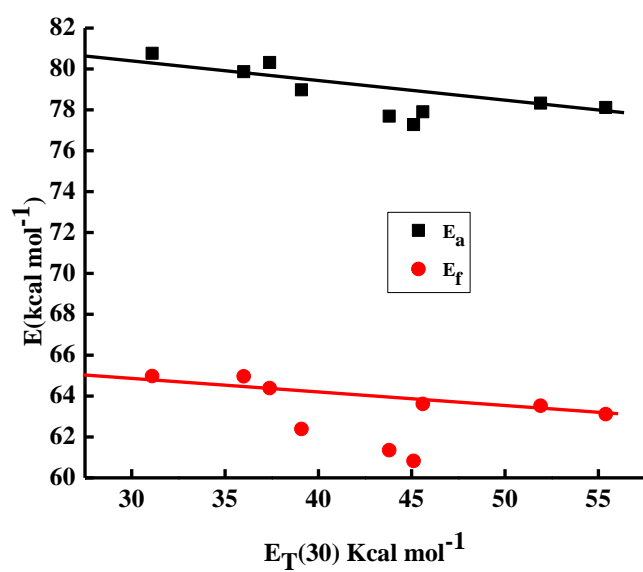
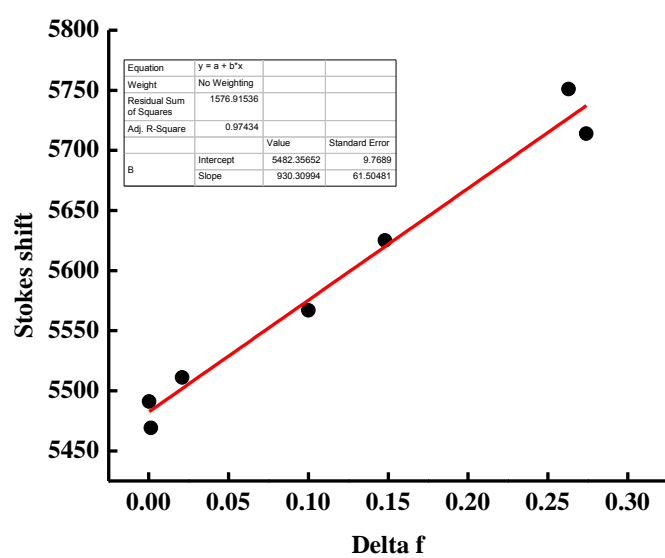**Fig. 4.** Plot of energy of absorption (E$_a$) and emission (E$_f$) versus E$_T$(30) of different solvents

Equation	y = a + b*x	
Weight	No Weighting	
Residual Sum of Squares	1576.91536	
Adj. R-Square	0.97434	
	Value	Standard Error
B Intercept	5482.35652	9.7689
Slope	930.30994	61.50481

Fig.5. Plot of Δ*f* versus Stokes shift (Δυ)
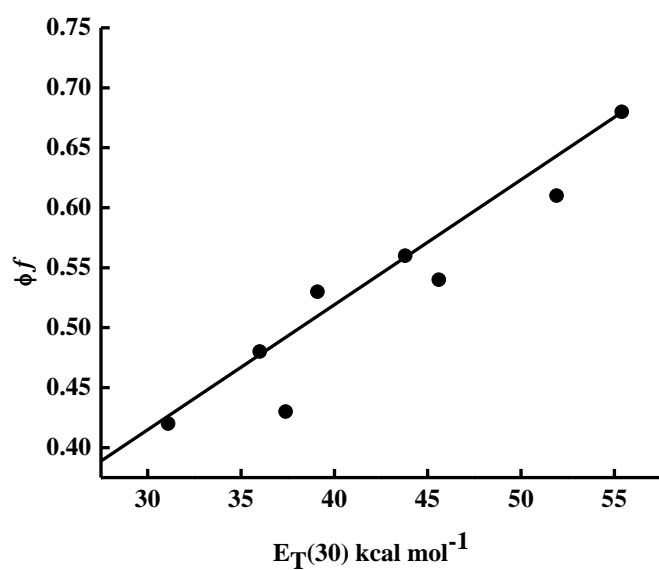
Fig.6. Plot of ϕ_f versus E_T (30) of different solvents.
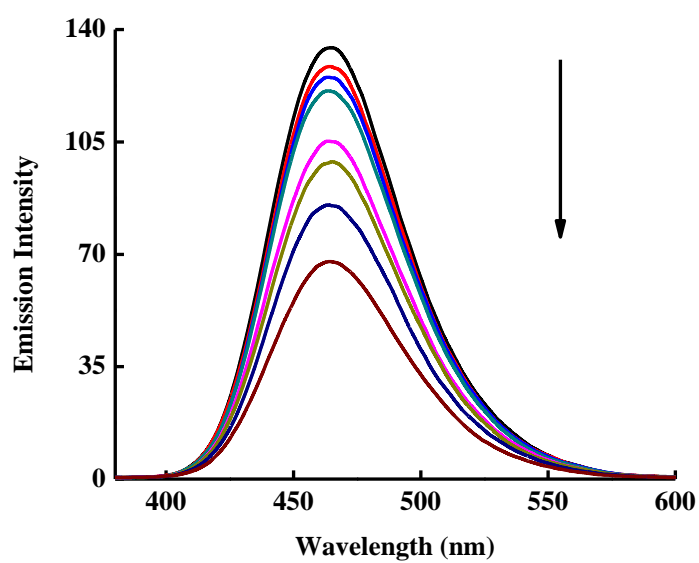
Fig. 7. Emission spectrum of 1×10^{-5} mol dm^{-3} of DPI at different concentrations of SDS, the concentrations of SDS at increasing emission intensity are 0.0, 2 x 10^{-3}, 4 x 10^{-3}, 6 x 10^{-3}, 8 x 10^{-3}, 10 x 10^{-3}, 12 x 10^{-3}, 16 x 10^{-3} and 18 x 10^{-3} mol dm^{-3}.
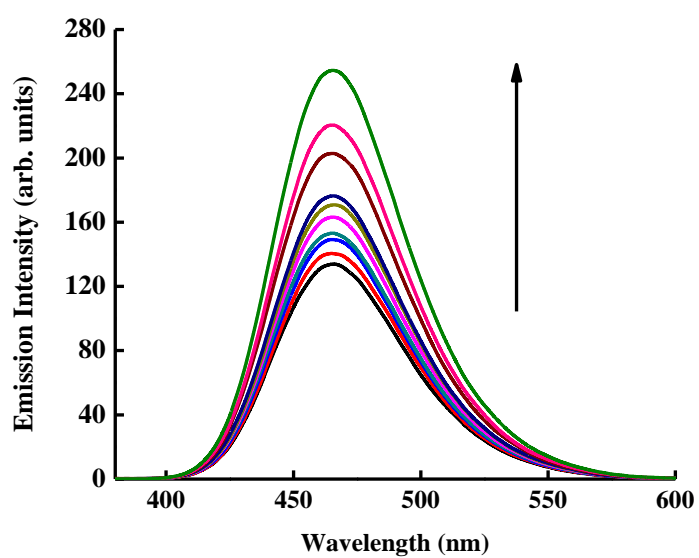
Fig 8. Emission spectrum of 1×10^{-5} mol dm^{-3} of DPI at different concentrations of CTAB, the concentrations of CTAB at increasing emission intensity are 0.0, 2×10^{-4}, 4×10^{-4}, 6×10^{-4}, 8×10^{-4}, 10×10^{-4}, 12×10^{-4}, 16×10^{-4} and 18×10^{-4} mol dm^{-3}.
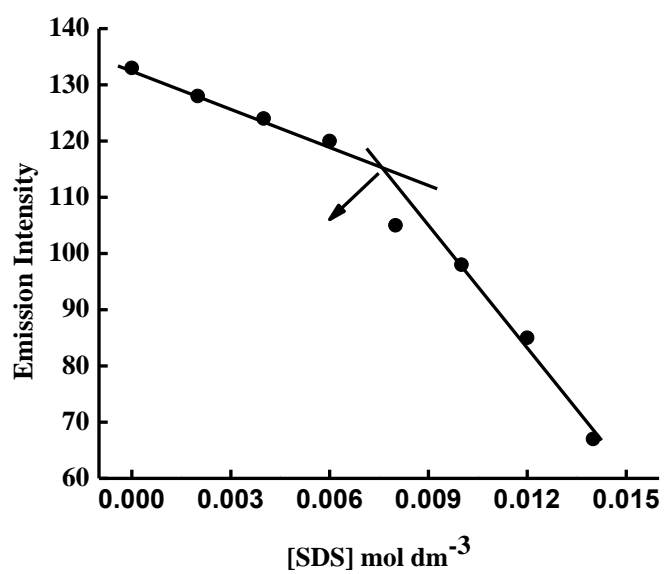
Fig. 9. Plot of I_f versus the concentration of SDS
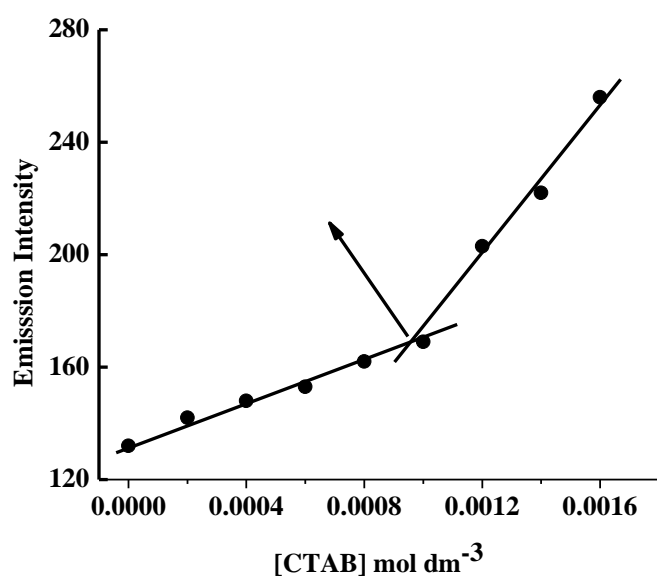
Fig. 10. Plot of I_f versus the concentration of CTAB
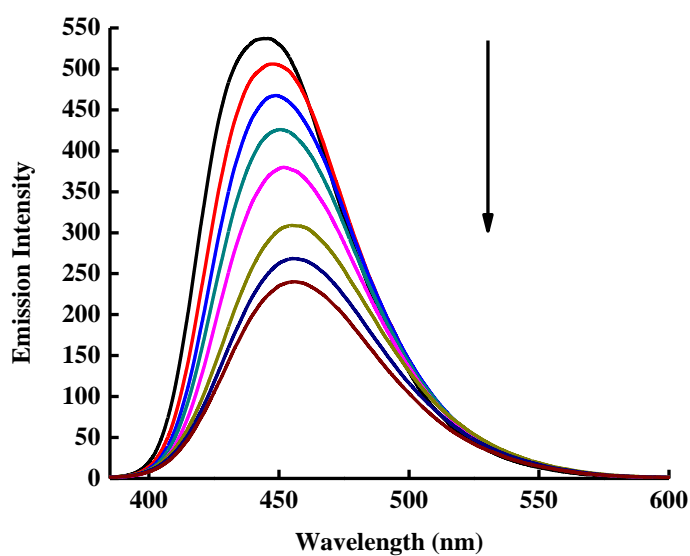
Fig. 11. Fluorescence quenching of 1×10^{-5} mol dm^{-3} DPI in dioxan by (λ_{ex} = 365 nm) by ethylene glycol, the concentration of ethylene glycol at decreasing emission intensity are 0, 0.35, 0.71, 1.06, 1.42, 1.72, 2.11, 2.49 and 2.84 mol dm^{-3}.
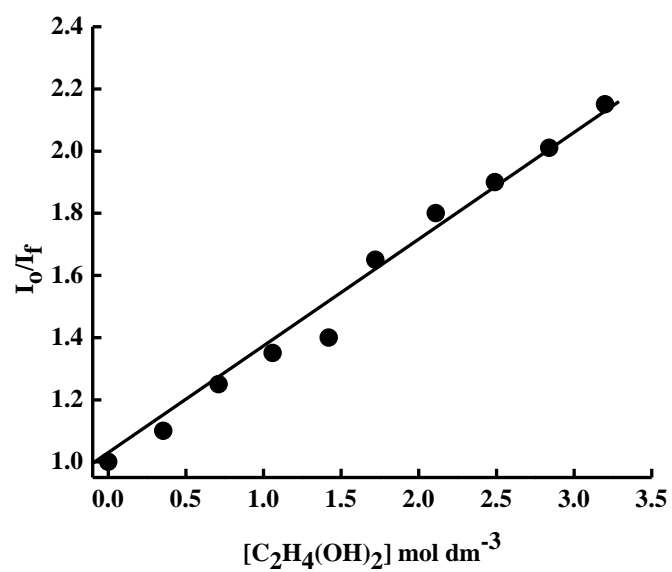
Fig. 12. Stern–Volmer plot of fluorescence quenching of 1×10^{-5} mol dm^{-3} of DPI in Dioxan by ethylene glycol
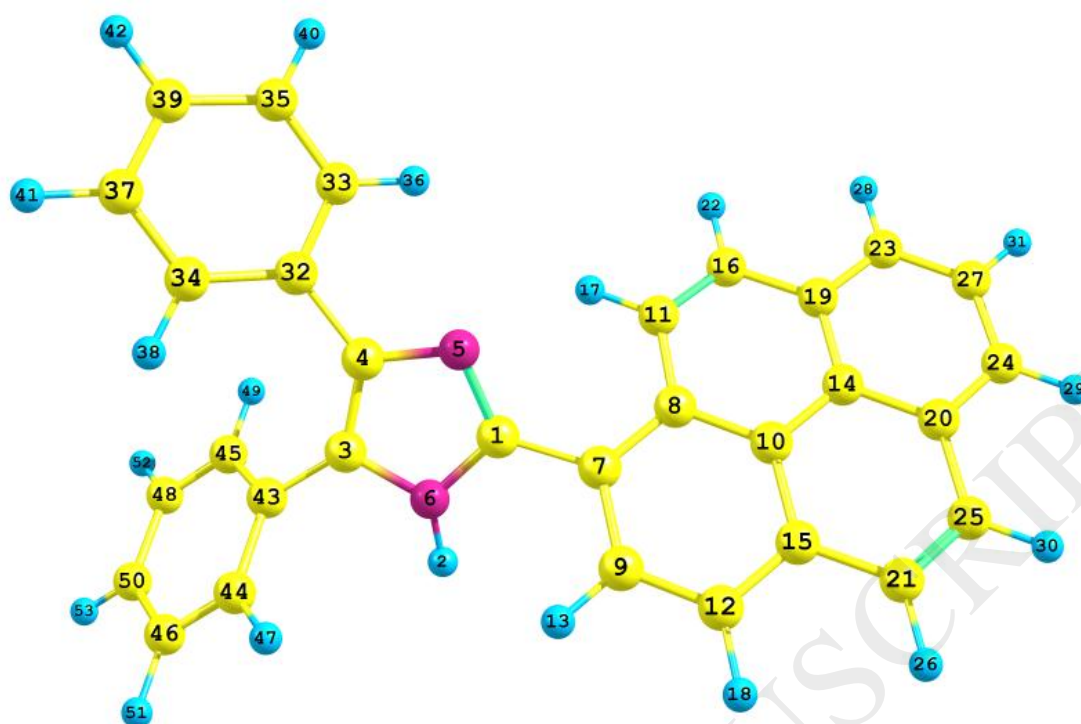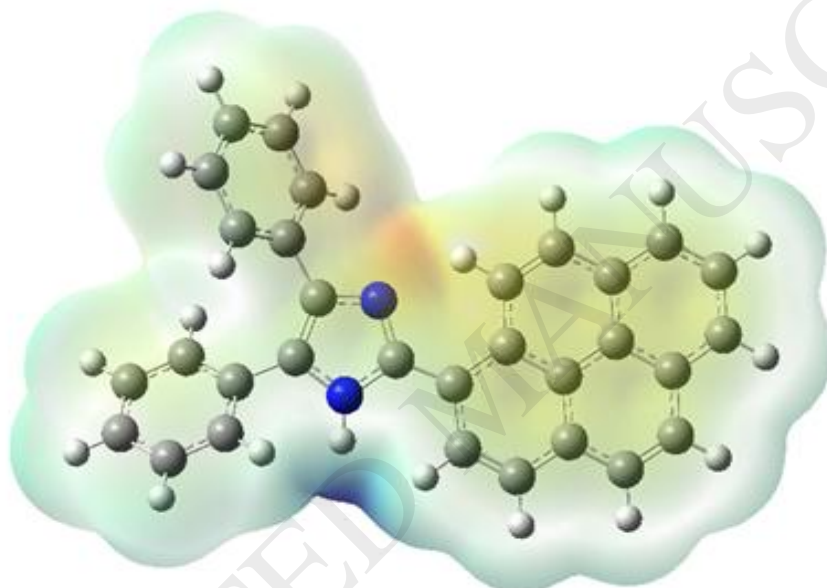
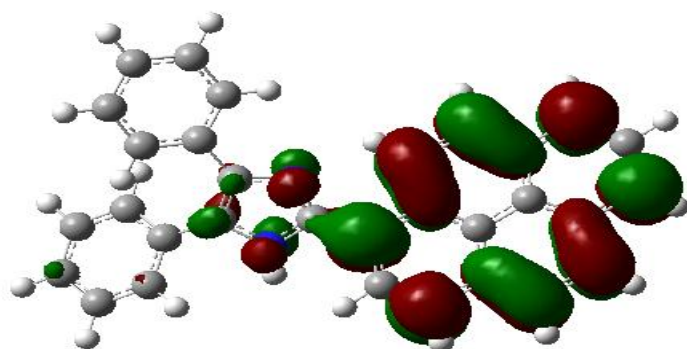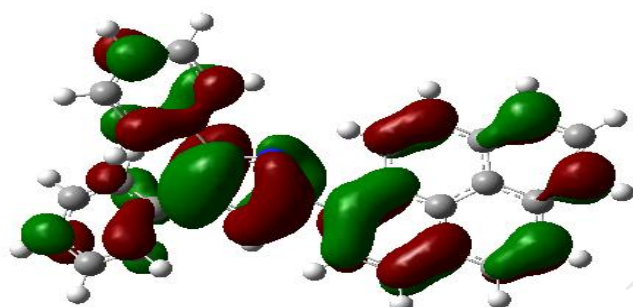**Fig.13** The atom numbering of DPI macromolecule.
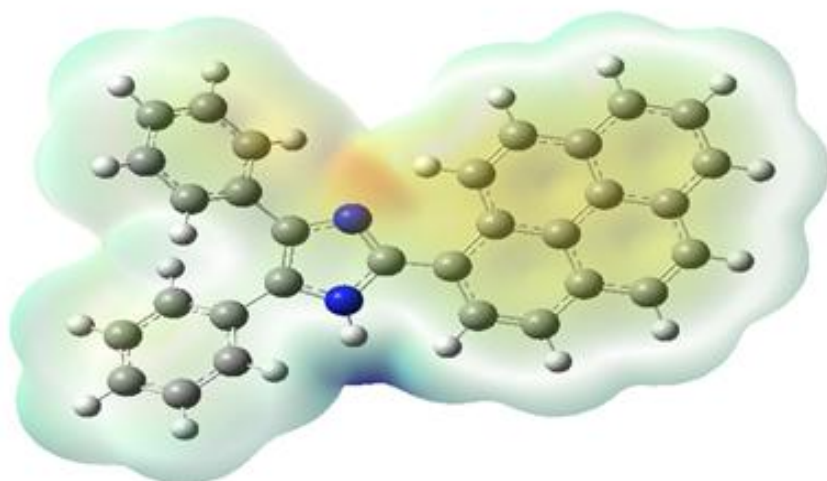
(a) Excited State

(b) Ground State

Fig.14 The mapped electrostatic potential for (a) excited and (b) ground states of gas-phase DPI which have been obtained by using HF/321Glevel of theory. They show the relatively negative values around the carbonyl group and the positive charges around the hydroxyl group.

43

LUMO

HOMO

Fig.15 The HOMO and LUMO of DPI which have simulated by using CAM-B3LYP/631+G* level of theory.